Analysis and Optimization of Air-Core Permanent Magnet Linear Synchronous Motors with Overlapping Concentrated Windings for Ultra-precision Applications

Liyi Li *, Yongbin Tang *, Mingna Ma* and Donghua Pan *

Abstract –This paper presents the analysis and optimization of air-core permanent magnet linear synchronous motor with overlapping concentrated windings to achieve high thrust density, high thrust per copper losses and low thrust ripple. For the motor design, we adopt equivalent magnetizing current (EMC) method to analyze the magnetic field and give analytical formulae for calculation of motor parameters such as no-load back EMF, dynamic force, thrust density and thrust per copper losses. Further, we proposed a multi-objective optimization by genetic algorithm to search for the optimum parameters. The design optimization is verified by 2-D Finite Element analysis (FEA).

Keywords: Air-core, Thrust density, Thrust per copper losses, Optimization

1. Introduction

Air-core permanent magnet linear synchronous motors (PMLSM) are gradually used in the field of ultra-precision application, such as ultra-precision measurement, precision two-dimensional drive system and IC manufacturing which must require high speed, high acceleration, rapid response, extremely low copper loss and precise positioning [1].

Recently, some researchers have been concerned about the analysis and optimization of air-core PMLSM. A design and analysis framework for the general class of surface-mounted permanent magnet linear machines have been presented in [2]. The motor fields, forces, flux linkage and inductance of the winding are given via the magnetic vector potential. Comparison of the thrust per copper losses of the machines has been done by deriving thrust per copper-mass factors for the different windings [3]. Non overlapping windings have certain important advantage compared to overlapping windings in the field of lower copper mass. The design optimization has been performed on an air-core linear motor to achieve high developed thrust and reduced magnet volume separately by choosing the shape and dimensions of coils and PMs as design variables [4]. A multi-objective design optimization has been proposed to improve thrust, thrust ripple and consumed magnet volume independently and simultaneously by genetic algorithm [5]. Harmonic contents of permanent magnet (PM) field have

been used to characterize thrust ripple, and yet the method is only suitable for a fixed coil structure and size [6]. However, for the ultra-precision application, the quality and volume of the motors must be strictly limited, and heat losses can affect some material deformation and the accuracy of the laser interferometer. Therefore, improvements of thrust per volume, thrust per copper losses and thrust ripple are required simultaneously to improve motor performance and adaptability.

In the paper, we give analytical formulae for its magnetic field, no-load back EMF, thrust per volume, thrust per copper losses and thrust ripple by Space Harmonics Field analysis. Further, shape and dimensions of coils and PMs are chosen as design variables. An objective function with weight coefficients is defined including thrust per volume, thrust per copper losses and thrust ripple. The motor dimensions are optimized using analyzed parameters based on the genetic algorithm method. The validity of the proposed technique is confirmed with 2-D FEA.

2. Machine Modeling

2.1 Motor Topologies

A schematic view of a double sided air-core PMLSM studied in this paper is presented in Fig. 1. The primary motor is a three-phase air-core overlapping concentrated windings. Each secondary consists of back-iron and PMs facing the primary windings.

  *   Electrical Engineering Department, Harbin Institute of Technology, China. (liliyi@hit.edu.cn,tangyongbin0622@163.com, mamingna1986@163.com, smile82812@163.com)
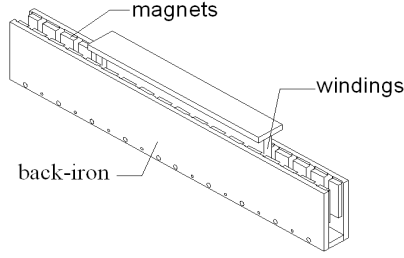
Fig. 1. Schematic view of air-core PMLSM

2.2 Motor Topologies

Since the double sided air-core PMLSM has a symmetric structure along the y-axis, only one side is selected as the analysis model. Fig. 2 shows a layer model of the machine with overlapping windings composed of 2 poles and 3 virtual slots. To simplify the two-dimensional analysis, it is assumed that:

(1) all regions are extended infinitely in the ±x direction;
(2) permeability of back iron is equal to infinity;
(3) the permeability of permanent magnets is equal to the permeability of free space.

For the theoretical aspects of this paper, we adopt Equivalent Magnetizing Current (EMC) method to describe the magnetic field distribution of magnets [2], [6]. PMs are replaced by the EMC distribution and equivalent to the current surface.
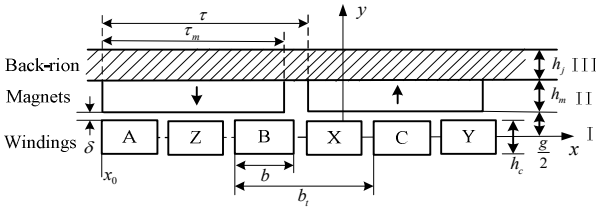

Fig. 2. Layer analysis model of air-core PMLSM

The magnetization of permanent magnet by a Fourier series is as follows [7]

$$M(x) = \sum_{n=1}^{\infty} \frac{4B_r}{\mu_0 \tau m_n} \sin \frac{m_n \tau}{2} \sin \frac{m_n \tau_m}{2} \sin m_n x \qquad (1)$$

where m_n is the spatial frequency which contains only odd harmonics

$$m = \frac{(2n-1)\pi}{\tau} \qquad (2)$$

where B_r, μ_0, τ, and τ_m are residual magnetization, the free space permeability, pole pitch and magnet width, respectively.

The Maxwell equations lead to Poisson equations as follows:

$$\begin{cases} \dfrac{\partial^2 A_1}{\partial x^2} + \dfrac{\partial^2 A_1}{\partial y^2} = 0 & \text{Re} \, gion \, \text{I} \\[3mm] \dfrac{\partial^2 A_2}{\partial x^2} + \dfrac{\partial^2 A_2}{\partial y^2} = -\mu_0 \overrightarrow{J_m} & \text{Re} \, gions \, \text{II} \end{cases} \qquad (3)$$

where A_1 is the vector potential of coils and air gap, and A_2 stands for the magnetic vector potential. Boundary conditions are as follows:

$$\begin{cases} H_{x2}\big|_{y=\frac{g}{2}} = H_{x1}\big|_{y=\frac{g}{2}} & H_{x2}\big|_{y=\frac{g}{2}+h_m} = 0 \\[3mm] H_{x1}\big|_{y=0} = 0 & B_{y1}\big|_{y=\frac{g}{2}} = B_{y2}\big|_{y=\frac{g}{2}} \end{cases} \qquad (4)$$

Using the above boundary conditions, the flux density induced by the PMs can be obtained as follows, respectively.

$$\begin{cases} B_{x1} = \sum_{n=1}^{\infty} m_n \left(A_{n1} ch m_n y + B_{n1} sh m_n y \right) \cos m_n x \\[3mm] B_{y1} = -\sum_{n=1}^{\infty} m_n \left(A_{n1} sh m_n y + B_{n1} ch m_n y \right) \sin m_n x \end{cases} \qquad (5)$$

where C_n is the coefficient given by

$$C_n = \frac{4B_r}{\tau m_n^2} \sin \frac{m_n \tau}{2} \sin \frac{m_n \tau_m}{2} \qquad (6)$$

Constants of equation (5) can be found as follows

$$\begin{cases} A_{n1} = 0 \\[2mm] A_{n2} = C_n \sinh\left(m_n \frac{g}{2} \right) \\[2mm] B_{n1} = C_n \dfrac{\sinh(m_n h_m)}{\sinh\left[m_n \left(h_m + \frac{g}{2} \right) \right]} \\[4mm] B_{n2} = -C_n \dfrac{\sinh\left(m_n \frac{g}{2} \right) \cosh\left[m_n \left(h_m + \frac{g}{2} \right) \right]}{\sinh\left[m_n \left(h_m + \frac{g}{2} \right) \right]} \end{cases} \qquad (7)$$

where h_m and g are magnet height and actual air gap length.

2.3 Characteristic Analyses

2.3.1 No-load back EMF calculation

The layout and dimensions of air-core overlapping

windings is shown in Fig. 3. The flux linkage of a single turn at position I in the phase can be obtained as follows
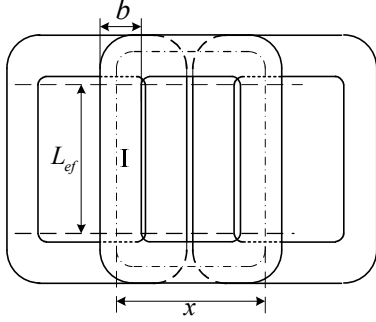

Fig. 3. Layout of air-core overlapping windings

$$\psi = \int B \bullet dS = \frac{1}{h_c} \int\limits_{vt+x}^{vt+1.5b_t+b-x} \int\limits_{-h_c/2}^{h_c/2} B_{y1} L dx dy \qquad (8)$$

where b_t, h_c, b and L are the slot distance of each coil, coil thickness, sided width of each coil and the effective width of the motor, respectively.

Assuming Ns is the number of conductor of every slot, the flux linkage of single ring winding is thus given by

$$\psi = -\sum_{n=1}^{\infty} \frac{4LN_s B_{n1}}{bh_c m_n^2} \sinh m_n \frac{h_c}{2} \sin m_n \left(vt + \frac{3b_t}{4} + \frac{b}{2} \right) \sin m_n \left(\frac{b}{2} \right) \sin m_n \left(\frac{3b_t}{4} \right) \qquad (9)$$

where $0 \leq x \leq b$ and $0 \leq b \leq b_t/2$.

Assuming a is the number of parallel circuits and Q is slot number, the No-load back EMF is thus given by

$$E_1 = -k_q \frac{Q}{3a} \frac{d\psi}{dt} \qquad (10)$$
$$= \sum_{n=1}^{\infty} \frac{8k_q LNvB_{n1}}{bh_c m_n} \sinh m_n \frac{h_c}{2} \cos m_n \left(vt + \frac{3b_t}{4} + \frac{b}{2} \right) \sin m_n \left(\frac{b}{2} \right) \sin m_n \left(\frac{3b_t}{4} \right)$$

where N and v are the number of conductor of each phase in series and the linear speed of the motor, respectively.

The distribution factor k_q in Equation (10) takes into account the effect on the back EMF when q coils are connected in series to form a coil group, and is given by

$$k_q = \frac{\sin \frac{q\varepsilon}{2}}{q \sin \frac{\varepsilon}{2}} \qquad (11)$$

where $\varepsilon = \pi - \frac{2p\pi}{Q}$.

2.3.2 Thrust Analysis

Armature reaction of air-core PMLSM is generally negligible due to large non-ferromagnetic air gap, and the saturation phenomenon of the main magnetic circuit currently does not exist owing to a non-core motor structure. Therefore, we use Lorentz' force law to gain electromotive thrust formulae by the flux density induced by PMs and the current density distribution of each phase.

$$dF_A = B_{y1} JL dx dy \qquad (12)$$

And S_f is the fill factor of the stator conductors given by

$$S_f = N_s A_d / 2bh_c \qquad (13)$$

where A_d is the cross-sectional area of one copper wire.

The current density of phases A, B, and C is as follows

$$\begin{cases} J_a = \sqrt{2}N_s I \sin(wt + \theta_0)/(2h_c b) \\ J_b = \sqrt{2}N_s I \sin\left(wt + \theta_0 + \frac{2\pi}{3}\right)/(2h_c b) \\ J_c = \sqrt{2}N_s I \sin\left(wt + \theta_0 - \frac{2\pi}{3}\right)/(2h_c b) \end{cases} \qquad (14)$$

where I, θ_0 and w are current RMS, the initial phase angle and the frequency, respectively.

The current density distribution of phase A is as follows

$$J_a(x) = \begin{cases} J_a & x_0 \leq x \leq x_0 + b \\ -J_a & x_0 + \frac{3b_t}{2} \leq x \leq x_0 + \frac{3b_t}{2} + b \end{cases} \qquad (15)$$

Similarly, the method is also suitable for phase B and phase C.

Therefore, thrust produced by phase A can be calculated

$$F_A = \sum_{n=1}^{\infty} H_1(n) \sin(wt + \theta_0) \cos m_n \left(x_0 + \frac{b}{2} + \frac{\tau}{2} \right) \sin\left(m_n \frac{b}{2} \right) \sin\left(m_n \frac{\tau}{2} \right) \qquad (16)$$

where the coefficient $H_1(n)$ is as follows

$$H_1(n) = 8\sqrt{2} B_{n1} pILS_f sh m_n \frac{h_c}{2} / (am_n A_d) \qquad (17)$$

where p is pole pair of the motor.

Similarly, the method can apply to phase B and phase C. Therefore, the whole electromotive thrust can be calculated by the synthesis of the thrust produced by each phase

$$F_1 = \sum_{n=1}^{\infty} H_1(n) \sin\left(m_n \frac{b}{2}\right) \sin\left(m_n \frac{\tau}{2}\right) \left(\sin\left(wt+\theta_0\right) \cos m_n \left(x_0 + \frac{b}{2} + \frac{\tau}{2}\right) + \right.$$
$$\left. \sin\left(wt+\theta_0+\frac{2\pi}{3}\right) \cos m_n \left(x_0 + \frac{b}{2} + \frac{7\tau}{6}\right) - \sin\left(wt+\theta_0-\frac{2\pi}{3}\right) \cos m_n \left(x_0 + \frac{b}{2} + \frac{5\tau}{6}\right) \right) \quad (18)$$

Since three-phase windings adopt star connection, the multiples of third harmonics components of flux density do not influence the machine performance. Therefore, an indirect measure of thrust ripple can be inferred as follows

$$TTR = \sqrt{\sum_{n=5,7,11\ldots}^{\infty} B_{yn}^2} \, / \, B_{y1} \quad (19)$$

2.3.3 Thrust Density Analysis

From the model in Fig. 2, the volume of the coupling part of the primary and the secondary is given by

$$V = 2p\tau\left(2\delta + h_c + 2h_m + 2h_j\right) L \quad (20)$$

where h_j and δ are the height of back-iron and the length of sided mechanical air gap. Assuming that λ is constant given by

$$\lambda = 2h_m + 2\delta + h_c \quad (21)$$

Therefore, the thrust per volume can be inferred as follows

$$\frac{F_1}{V} = \sum_{n=1}^{\infty} P(n) \sin\left(m_n \frac{b}{2}\right) \sin\left(m_n \frac{\tau}{2}\right) \left(\sin\left(wt+\theta_0\right) \cos m_n \left(x_0 + \frac{b}{2} + \frac{\tau}{2}\right) + \right.$$
$$\left. \sin\left(wt+\theta_0+\frac{2\pi}{3}\right) \cos m_n \left(x_0 + \frac{b}{2} + \frac{7\tau}{6}\right) - \sin\left(wt+\theta_0-\frac{2\pi}{3}\right) \cos m_n \left(x_0 + \frac{b}{2} + \frac{5\tau}{6}\right) \right)$$
$$(22)$$

where the *P(n)* coefficient is given by

$$P(n) = 4\sqrt{2} B_{n1} I S_f sh m_n \frac{h_c}{2} \, / \, \left(a\tau A_d m_n \left(\lambda + 2h_j\right)\right) \quad (23)$$

2.3.4 Thrust per Copper Losses Analysis

The allowed copper losses depend on the resistance, thermal resistance and cooling of the motor, with the fixed phase current.

The copper losses of the machine is as follows

$$P_{cu} = 3I^2 R \quad (24)$$

And R is the resistance per phase given by
$$R = \rho(L + L_e) N_s Q \, / \, (3\pi a^2 A_d) \quad (25)$$

where ρ is resistivity of copper.

For practical overlapping windings, L_e is set to

$$L_e = \delta\left(b_t - b\right) \quad (26)$$

where δ is constant for the fixed coil structure.

So the thrust per copper losses can be inferred as follows

$$\frac{F}{\sqrt{P_{cu}}} = \sum_{n=1}^{\infty} q(n) \sin\left(m_n \frac{b}{2}\right) \sin\left(m_n \frac{\tau}{2}\right) \left(\sin\left(wt+\theta_0\right) \cos m_n \left(x_0 + \frac{b}{2} + \frac{\tau}{2}\right) + \right.$$
$$\left. \sin\left(wt+\theta_0+\frac{2\pi}{3}\right) \cos m_n \left(x_0 + \frac{b}{2} + \frac{7\tau}{6}\right) - \sin\left(wt+\theta_0-\frac{2\pi}{3}\right) \cos m_n \left(x_0 + \frac{b}{2} + \frac{5\tau}{6}\right) \right) \quad (27)$$

where the *q(n)* coefficient is given by

$$q(n) = \frac{8p}{m_n} \sqrt{\frac{S_f \pi}{\rho Q b h_c}} \frac{L}{\sqrt{L+L_e}} B_{n1} sh m_n \frac{h_c}{2} \quad (28)$$

The analysis show thrust ripple, thrust density and thrust per copper losses are varied with dimensions of PMs and coils.

3. Optimal Design of ILPMSLM

In this section, an effective multi-objective optimization is carried out based on the analytical formulae presented in Section 2.

3.1 Optimization Problem

Optimization objectives in this paper include thrust density, thrust per copper losses and thrust ripple. An objective function with the general form is given by

$$f = \left(\frac{F}{V}\right)^m \bullet \left(\frac{F}{\sqrt{P_{cu}}}\right)^n \, / \, \left(TTR\right)^k \quad (29)$$

where weight coefficients *m*, *n* and *k* are chosen for designers to determine the relative importance of thrust density, thrust per copper losses and thrust ripple in the multi-objective optimization for different applications and operating conditions.

An optimization problem should include some objectives, variables, and constraints. Outline dimensions and phase current of the motors are limited via fixed variables shown in Table 1. The constant λ in equation (21) shows that the sum of magnet height, air gap length and coil thickness is a fixed numerical value.

Table 1. The fixed variables

Parameters (unit)	Symbol	Value
pole pair	p	8
elementary slot number	Q	24
pole pitch (mm)	τ	21
constant λ (mm)	λ	17
back-iron height (mm)	h_j	6
motor active length (mm)	L	60
sided mechanical air gap length (mm)	δ	0.7
slot distance (mm)	b_t	14
the number of parallel circuits	a	2
the fill factor of the stator conductors	S_f	80.6%
the cross- sectional area of one wire (mm^2)	A_d	0.22
current RMS(A)	I	7

To have a more realistic optimization, some constraints are applied to design variables listed in Table 2. Sided width of each coil is limited by an upper bound to be a little lower than half slot distance and by a lower bound to have an accepted thrust. Magnet width is limited by a lower bound to have an acceptable thrust density. Magnet height is limited by an upper bound to prevent saturation phenomenon and by a lower bound to have an accepted thrust.

Table 2. Design variables constraints

Variables (unit)	Symbol	Min	Max
Sided width of each coil (mm)	b	2	6.5
Magnet width(mm)	τ_m	8.4	21
Magnet height (mm)	h_m	3.4	6.8

Fig. 4 shows the variation of thrust with varying magnet width and magnet height. Fig. 5 shows the variation of thrust density with varying magnet width and coil sided width. Fig. 6 shows the change rule of thrust per copper Losses and magnet dimensions. It is shown that thrust per copper Losses realizes the maximization while magnet width is equal to 21mm and magnet height is equal to 5.4mm. Fig. 7 shows the variation of thrust per copper with varying magnet width and coil sided width. It is seen that both thrust and thrust per copper increase with increasing magnet width and coil sided width. It is shown that thrust increase with increasing magnet height. However, a maximization of thrust per copper Losses is aimed with a suitable magnet height. Therefore, to realize high thrust, low copper loss and high accuracy simultaneously in ultra-precision applications, we proposed a multi-objective optimization by genetic algorithm to search for the optimum parameters.
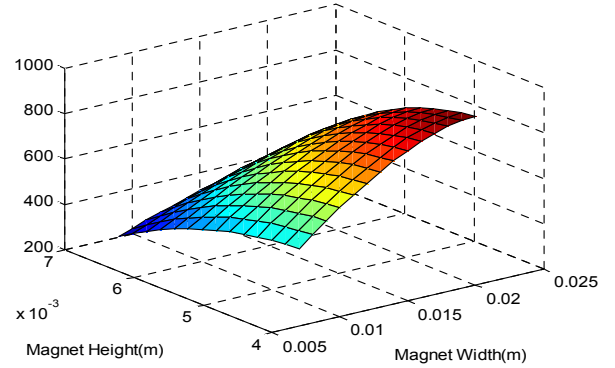

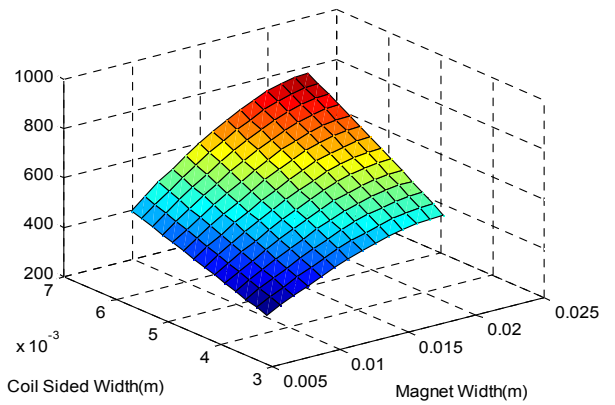**Fig. 4.** Variations of the force with magnet width and magnet height

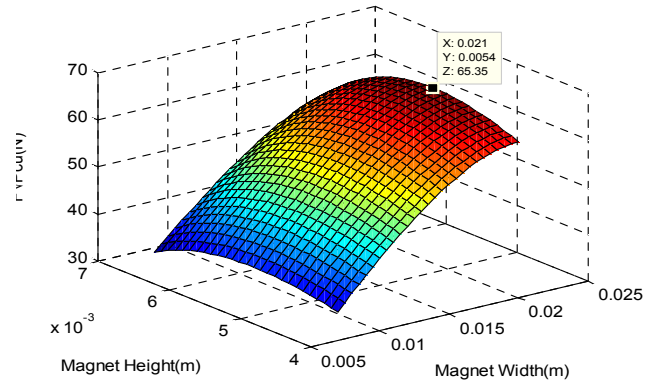**Fig. 5.** Variations of the force with magnet width and coil sided width

Fig. 6. Variations of thrust per copper Losses with magnet width and magnet height

3.2 Genetic Algorithm

The genetic algorithm provides a random search technique to find a global optimal solution in a complex multidimensional search space. The algorithm consists of three basic operators, such as selection, crossover and mutation. Table 3 shows the genetic algorithm parameters in this work.
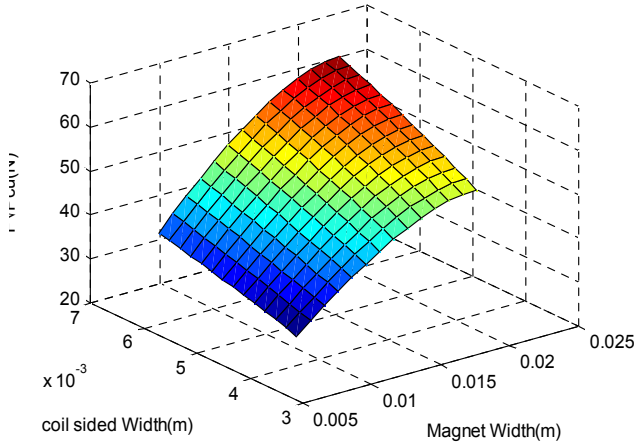
Fig. 7. Variations of thrust per copper Losses with magnet width and coil sided width

Table 3. Genetic algorithm parameters

Parameters	Value
Population size	100
Generations	1000
Crossover Fraction	0.75
Migration Fracion	0.2
Elite Count	20
Interval	20

3.3 Multi-objective Optimization

Moreover, in comparison with the original motor, design variables of the optimal motor for two different weight coefficients are shown in Table 4.

Table 4. Design variables for different weight coefficients

Variables (unit)	Symbol	The Original motor	*m=1.2 n=1.6 k=0.6*	*m=1 n=1 k=1*
Magnet height (mm)	h_m	4	5	4.3
Magnet width(mm)	τ_m	16	18	16.8
Sided width of coil (mm)	b	5.8	6.4	5.9

The results of the design optimization are listed in Table 5. When choosing *m*=1.2, *n*=1.6 and *k*=0.6, thrust density and thrust per copper losses improve remarkably, but thrust ripple also increase. However, considering the relative importance of thrust density, thrust per copper losses and thrust ripple for ultra-precision application, the optimal motor by choosing *m*=1, *n*=1 and *k*=1 increases thrust density by 11%, thrust per copper losses by 8.2% and reduces thrust ripple to 0.5% compared to the original motor.

Table 5. Results of the optimization for different weight coefficients

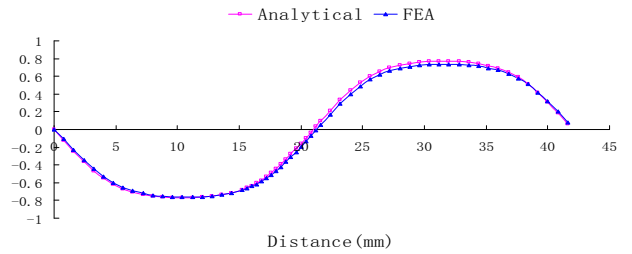| Parameters (unit)		The Original motor	*m=1.2 n=1.6 k=0.6*	*m=1 n=1 k=1*
Thrust(N)	Analytical	743	859	827
	FEA	724	840	825
Thrust Density (N/cm³)	Analytical	1.18	1.37	1.31
Thrust per copper losses (N/sqrtW)	Analytical	51.6	62	55.9
Thrust ripple	Analytical	0.7%	0.8%	0.4%
	FEA	0.8%	0.9%	0.5%

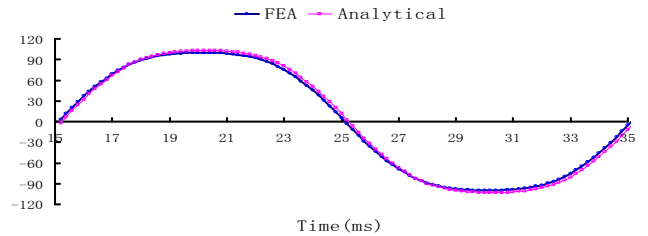**Fig. 8.** Flux density distribution at the centre of air gap

Fig. 9. No-load back EMF

3.4 Optimization Evaluation

The multi-objective design optimization was discussed based on the analytical model presented in section 2. The analytical formulae showed up changing regularities of its magnetic field, dynamic thrust, thrust density and thrust per copper losses with varying the motor parameters, especially dimensions of magnet and coils. However, in order to simplify the analytical model, armature reaction and saturation were ignored. Therefore, it is necessary to evaluate the accuracy of the analytical formulae. Fig. 8 shows the compare results of the flux density by PM at the centre of air-gap. The maximum error in the case of the flux density calculation is less than 3%, which is reasonable. Fig. 9 shows the comparison of no-load back EMF by analytical methods and FEA. The maximum error in the case of the no-load back EMF is less than 3%, which is

acceptable. In this work, the compare results of developed thrust, copper losses and thrust ripple are shown in Table V. It is seen that the results of theoretical analysis are very close to the results of 2D-FEA. These indicate the validity of the multi-objective optimization.

4. Conclusion

In this paper, the analytical model and formulae based on Maxwell equations were derived to predict the magnetic field, thrust, thrust density, thrust per copper losses and thrust ripple of air-core PMLSM with overlapping windings. The characteristic analysis of the motors reveal change rules of thrust density, thrust per copper losses and thrust ripple with varying shape and dimensions of magnets and coils.

A genetic algorithm based on the analytical formulae proposed in section II is carried out to search for the optimal design variables. Keeping the same outline dimensions and phase current of the motors, the optimal motor simultaneously increases thrust density by 11%, thrust per copper losses by 8.2% and reduces thrust ripple to 0.5% compared to the original motor. Finally, the analytical results of the multi-objective optimization were verified by 2-D FEA results.

Acknowledgements

References

[1] N. Fojii and K. Okinaga, "X-Y Linear Synchronous Motor without Force Ripple and Core Loss for Precision Two-dimensional Drive," *IEEE Trans. Magn.*, vol. 38, no. 5, pp. 3273–3275, Sep. 2002.

[2] David L. Trumper, Won-jong Kim, and Mark E. Williams, "Design and Analysis Framework for Linear Permanent-magnet Machines," *IEEE Trans. Ind. Applicat.*, vol. 32, pp. 371–379, 1996.

[3] M.J. Kamper, "Comparison of Linear Permanent Magnet Machine with Overlapping and Non-overlapping Air-cored Stator Windings", *4th International Conference on Power Electronics, Machines and Drives (PEMD)*, York (UK), April 2008.

[4] S. Vaez-Zadeh and A. R. Ghasemi, "Design Optimization of Permanent Magnet Synchronous Motors for High Torque Capability and Low Magnet Volume," *Elect. Power Syst. Res*, vol. 74, pp. 307--313, Mar. 2005.

[5] S. Vaez-Zadeh, and A. H. Isfahani, "Multi-objective Design Optimization of Air-core Linear Permanent-Magnet Synchronous Motors for Improved Thrust and Low Magnet Consumption," *IEEE Trans. Magn.*, vol. 42, no. 3, pp. 446-452, March 2006.

[6] Gyu-Hong Kang, Jung-Pyo Hong, and Gyu-Tak Kim, "A Novel Design of an Air-core Type Permanent Magnet Linear Brushless Motor by Space Harmonics Field Analysis," *IEEE Trans. Magn.*, vol. 37, no. 5, pp.3732-3736, September 2001.

[7] Koen J. Meessen, Bart L. J. Gysen, Johannes J. H. Paulides, and Elena A. Lomonova, "Halbach Permanent Magnet Shape Selection for Slotless Tubular Actuators ," *IEEE Trans. Magn.*, vol. 44, no. 11, pp. 4305–4308, November 2008.

Liyi Li received Ph.D. degrees in electrical engineering from Harbin Institute of Technology, Harbin, China, in 2001. His research interests are design and control of electrical machines.

Yongbin Tang received the B.E. degree in 2007 and the M.E. degree in 2009 from Harbin Institute of Technology, Harbin, China. He is currently with the Institute of Electromagnetic and Electronic Technology, Harbin Institue of Technology as a doctoral candidate from 2009. His research areas are design and control of permanent magnet linear synchronous motor.

Mingna Ma received the B.E. degree in 2007 and the M.E. degree in 2009 from Harbin Institute of Technology, Harbin, China. She is currently with the Institute of Electromagnetic and Electronic Technology, Harbin Institute of Technology as a doctoral candidate from 2009. Her research areas are magnet linear synchronous motor and linear electromagnetic launcher.

Donghua Pan received the B.E. and M.E. degrees from Shenyang University of Technology, Shenyang, China, in 2005 and 2008, respectively. He has been working toward the Ph. D. degree in the Institute of Electromagnetic and Electronic Technology, Harbin Institute of Technology, Harbin, China, since 2008. His research areas are permanent magnet linear synchronous motor and voice coil motor.